Article

Study of a methodology for calculating contact stresses during blade processing of structural steel

Victor Kozlov[1], Artem Babaev[2]*, Nikita Schulz[2], Artem Semenov[2], Anton Shevchuk[2]

[1]- Division for Mechanical Engineering, National Research Tomsk Polytechnic University, 634050 Tomsk, Russia

[2] Scientific and Educational Center "Additive Technologies", National Research Tomsk State University,
634050 Tomsk, Russia

* Correspondence: temkams@mail.ru

Abstract: The article presents data about the distribution of contact stresses on the rake surface of the cutter when turning steel (Fe-0.4 C-1Cr), which were obtained by the split cutter method. The article also provides graphs of the effect of the uncut chip thickness *a* and the rake angle γ on the main parameters of the plots of shear τ and normal σ contact stresses. For this case, The initial data were obtained by longitudinal turning of a steel workpiece with the measurement of the technological components of the cutting force by a three-component Kistler dynamometer, followed by the calculation of the physical components of the cutting force. These components were used to construct contact stress diagrams taking into account the epures (plots) obtained by the split cutter method (method of a sectional tool). The rake angle varied widely: from +35 to -10 °, and the uncut chip thickness *a*: from 0.05 to 0.37 mm. At the first half of the chip contact with the rake surface of the cutter, i.e. from 0 to 0.5 of the total contact length *c*, uniformly distributed contact shear stresses $\tau \approx const \approx 350\text{-}550$ (MPa) act, which indicates the plastic nature of the contact at this area. The magnitude of the greatest shear contact stress $\tau_{max} = \tau_{const}$ with a decrease in the uncut chip thickness *a* varies slightly (from 350 to 400 MPa) in the range $a = 0.37\text{-}0.05$ mm and the rake angle $\gamma = +35\text{-}0$ °, but the larger the rake angle, the greater the value of τ_{max}. A decrease in the rake angle from +35 to -10° leads to a significant increase in the maximum normal contact stress at the cutting edge σ_{max}: from 400 to 1400 MPa with the uncut chip thickness $a = 0.37$ mm. In the area of small uncut chip thickness, *a* (less than 0.1 mm), the paradoxical increase in the magnitude of the greatest normal contact stress with a large positive rake angle (more than +15 °) is explained by the indentation (pressing) of the being machined material under the rounded cutting edge of the cutter in the chip formation zone, and their paradoxical decrease with a negative rake angle is due to the presence of a sag (deflection) of the transient surface. According to the magnitude of the reference points obtained on the basis of experimental data, it is possible to plot the contact stresses epures on the rake surface of the cutting tools when machining steel.

Keywords: contact loads; contact stresses; steel machining; split cutter method; strength of cutting tools.

Citation: To be added by editorial staff during production.

Academic Editor: FirstnameLastname

Received: date
Revised: date
Accepted: date
Published: date

1. Introduction

Calculating the strength of a cutting tool requires knowledge of not only the components of the cutting force, but also the distribution of contact stresses (contact loads) on the rake and rear surfaces [1, 2]. This task is especially important when machining dificalt-to-machining (hard-to-machining) materials [13, 16, 20, 26, 28-30] and for roughing with a

worn tool, when a chipping of the cutting edge or destruction of the cutting plate may occur [1-10, 18].

Experimental and analytical methods are still the main ways to study various types of cutting tool wear. Calculations performed by the finite element method show the prediction of the magnitude of cutting forces in the process of blade processing [15, 17, 19]. Numerous developments in numerical methods and simulations associated with the existence of increasingly powerful computers make it possible to study tool wear using FEM. Modeling issues are addressed by considering microstructures as homogeneous characteristics and corresponding verification methods [27, 34-36].

Tool condition monitoring is an important part of tool prediagnosis and condition management systems. Accurately predicting tool wear is essential to fully utilize tool life, improve production efficiency and product quality, and reduce tool costs. There are various methods for diagnosing the condition of a cutting tool –cutting force measurement, temperature signals, automated vibration diagnostic data collection systems, real-time studies of wear and abrasion of the cutting edge, and others [14, 21, 22-25, 31-33, 36].

The most dangerous is the wear of the flank surface with appearance of a chamfer on the side-relief surface (flank-land) with a length h_f (Figure 1, 2) and large contact loads leading to tool failure.

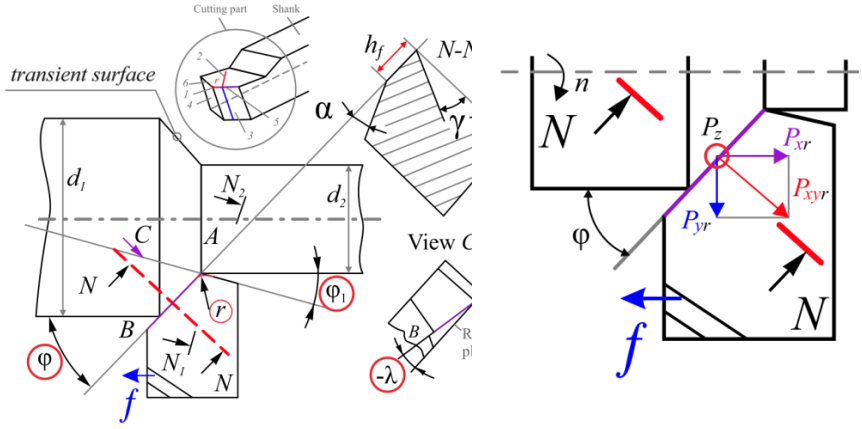

(a) (b)

Figure 1. Top view (a) and cross section of the cutter in the major orthogonal plane N-N (b).

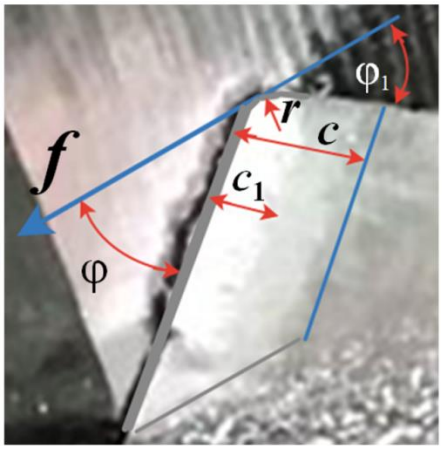

Figure 2. The principal edge angle in the plan **φ**, the nose radius ***r***, the total contact length ***c*** and the length of plastic contact c_1 of a chip with a rake surface of a cutter, instrumental portable microscope.

The method of a "section tool" (or split cutter method) is used for research of contact stresses distribution (Figure 3 and 4) [10-12]. It is very labour-consuming, demands use of rigid special four-component dynamometer, and in cutting difficult-to-machinematerial occurs chipping and breakage of cutting plates which causes the repetition of all series of experiments. Therefore, we had carried out research on the calculation of epures'parametres of contact stresses which use the measured or calculated technological components of cutting force.

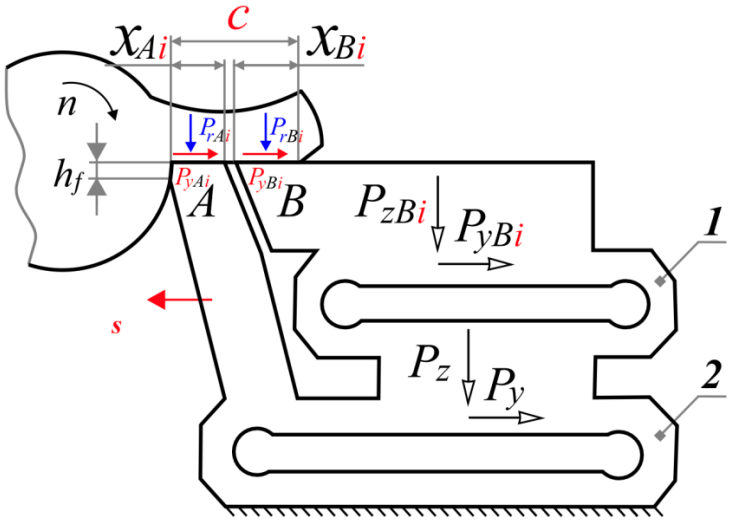

Figure 3. The position of the plates ***A*** and ***B*** of the split cutter when the chips come into contact with the main measuring plate ***B*** in a section of length x_{Bi} and width ***b***.

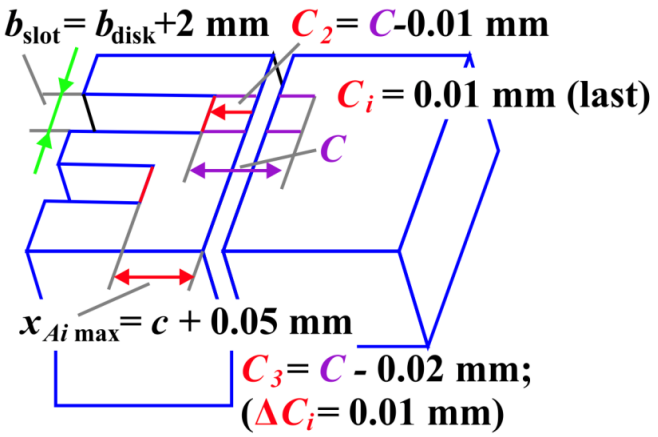

Figure 4. Sections of the split cutter.

2. Materials and Methods

The study of the contact stresses distribution was performed when turning a workpiece made of steel (Fe-0.4 C-1 Cr, or steel 5140 in accordance to ASTM-SAE) with hardness HB 180 and ultimate tensile stress σ_{UTS}=495 MPa by two different methods:

1. First using the split cutter method (Figure 3 and 4) to determine the distribution (epure, plots) of contact stresses on the rake (front) surface of the cutter, followed by the determination of the parameters of the characteristic (reference) points of the contact stress plots (epure). This will make it possible to plot the normal σ and shear (tangential) τ contact stresses (MPa) according to the normal ***N*** and

shear (tangential) F physical components of the cutting force P_r (N) on the rake surface. These forces can be calculated by knowing the measured technological components $P_{z\,r}$ and $P_{xy\,r}$ of the cutting force and the magnitude of the rake angle γ. The use of the split cutter method also makes it possible to determine the distribution (epure, plots) of normal σ_h and shear (tangential) τ_h contact stresses (MPa) on the wear chamfer on the side-relief (rear) surface (on the flank-land surface);

2. With the measurement of the technological components $P_{z\,r}$ and $P_{xy\,r}$ of the cutting force on the rake surface of the cutter during longitudinal turning of the workpiece with a conventional turning cutter, followed by the calculation of the normal N and shear (tangential) F of the physical components of the cutting force P_r on the rake surface. Based on these physical components of the cutting force on the rake surface, distribution (epure, plots) of normal σ and shear (tangential) τ contact stresses on the rake surface were constructed, taking into account the regularity (rules) that were obtained by the split cutter method.

Since measuring the technological components of the cutting force using a conventional three-component turning dynamometer is less laborious compared to using a special four-component dynamometer for the split cutter method [1], measurements were performed with a large number of experiments with different cutting modes and the rake angle of the turning cutter.

This made it possible to identify the influence of the above conditions on the magnitude of the main parameters of the contact stress plots, according to which it is possible to construct plots for the studied conditions without performing experiments.

When performing experiments using the split cutter method, a special dynamometer designed by V.A. Krasilnikov [10, 11] was used, having two levels (frames) of elastic measuring elements 1 and 2 (Figure 3), which allows controlling the constancy of the common technological components P_z and P_y of the cutting force, regardless of length the chip section x_{Bi}, which is in contact with the main measuring plate B.

The cutting of the periphery of the disk made from the have being machined material was carried out with a radial feed rate of the cutter $f = f_{rad,\,T}$, i.e. with orthogonal (rectangular) free cutting, therefore the uncut chip thickness a (mm) is equal to the feed rate f_{rad} (mm/rev).

Plates with a width of 120 mm have several sections in which the different distance x_{Ai} (mm) from the cutting edge to the surface that separates the plates (Figure 4). In the manufacture of plates, the largest distance $x_{Ai\,max}$ is slightly longer than the chip contact length with the rake surface of the cutter c (mm), which corresponds to the material have being machined, rake angle and the selected cutting mode: feed rate f (mm/rpm) and cutting speed v (m/min).

The have being machined disk with the diameter $d_{disk} = 250…180$ mm (Figure 5) is pre-prepared for the experiment: it is machined on the peripheral part for a short length of 15-20 mm from the periphery on diameter and with width $b_d = 4$ mm to increase the rigidity of its working part and reduce its broadening in contact with the cutting edge of the cutter. The width of the uncut chip b (mm) was assumed to be equal to the width of the disk b_d (mm) due to a slight broadening of the chips during cutting.

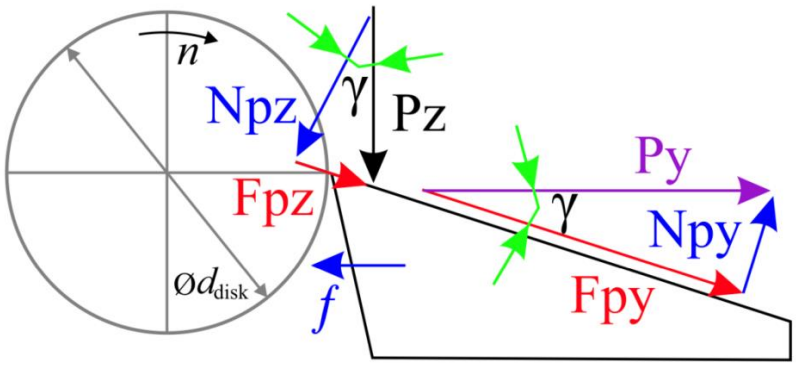

Figure 5. Diagram of the direction of the components of technological P_z, P_y and physical N_{Pz}, F_{Pz}, N_{Py}, F_{Py} cutting forces on the rake (front) surface of the cutter in the major orthogonal plane with rectangular free turning of the periphery of the disk at a positive rake (front) angle γ.

When the contact area of the cutting edge with the disc changes, i.e. when the cutter periodically moves along the axis of rotation of the disc, the distance x_{Ai} changes (Figure 3 and 4), but the sum of the length of the chip contact with the rake surface of the plate A (x_{Ai}) and plate B (x_{Bi}) remains unchanged: $x_{Ai} + x_{Bi} = c$.

The calculation of the physical components of the cutting force N and F according to the technological components P_z and P_y when the rake (front) angle $\gamma \neq 0°$ is performed according to the formulas that were obtained from the sum of the vectors (Figure 5):

$$\vec{P}_z = \vec{N}_{Pz} + \vec{F}_{Pz};\ \vec{P}_y = \vec{F}_{Py} + \vec{N}_{Py}.$$

From these formulas, when $\gamma > 0°$, we obtain two equations (1) and (2) for calculating the physical cutting forces:

$$N = N_{Pz} - N_{Py} = P_z \times \cos\gamma - \mathbf{P_y \times \sin\gamma}, \quad (1)$$

$$F = F_{Py} + F_{Pz} = P_y \times \cos\gamma + P_z \times \sin\gamma \quad (2)$$

In equation (1), the second term has a minus sign ($-N_{Py}$), since this component is directed in the opposite direction compared to the direction of the N_{Pz} vector. This creates a paradoxical situation: with an increase in the rake angle γ with an increase in the technological force P_y, the normal physical force N in equation (1) decreases, which at very large rake angles (more than 25 °) can lead to a small normal force N if the second part of formula (1) is only slightly less than the first part, i.e. the average conditional coefficient of friction $\mu_{average} = F/N$ will increase with an increase in the rake angle γ.

With a negative value of the rake angle γ and non-free cutting, slightly different equations are used:

$$\mathbf{N = N_{Pz} + N_{Pxy} = P_z \times \cos\gamma + P_{xy} \times \sin\gamma}, \quad (3)$$

$$\mathbf{F = F_{Pxy} - F_{Pz} = P_{xy} \times \cos\gamma - P_z \times \sin\gamma}. \quad (4)$$

where $\mathbf{P_{xy} = (P_x^2 + P_y^2)^{0,5}}$.

The increment of the forces P_y and P_z on the considered i-th section of the plate in comparison with these forces on the previous (i-1) section are calculated by the equations:

$$\Delta P_{y\,B\,i} = P_{y\,B\,i} - \Delta P_{y\,B\,i-1}(\mathrm{H}). \quad (5)$$

$$\Delta P_{z\,B\,i} = P_{z\,B\,i} - \Delta P_{z\,B\,i-1}\ (H). \quad (6)$$

The normal N_i and shear (tangential) $F_i$forces acting on the i-th section are calculated according to equations (7) and (8) in accordance with equations (1), (2) and (5), (6):

$$N_i = \Delta P_{z\,B\,i} \times \cos\gamma - \Delta P_{yBi} \times \sin\gamma, \quad (7)$$

$$F_i = \Delta P_{yBi} \times \cos\gamma + \Delta P_{z\,B\,i} \times \sin\gamma. \quad (8)$$

The specific normal $q_{N\,i}$ and shear (tangential) $q_{F\,i}$ contact loads (forces) on the i-th section of plate B are calculated as the ratio of the increment of forces on this section to the increment of the chip contact area ΔS_i on this i-th section:

$$q_{N\,i} = \Delta N_i / \Delta S_i = (N_i - N_{i-1})/(\Delta x_i \times b) \quad \text{(MPa)}; \quad (9)$$

$$q_{F\,i} = \Delta F_i / \Delta S_i = (F_i - F_{i-1})/(\Delta x_i \times b) \quad \text{(MPa)} \quad (10)$$

At $\Delta x_i \to 0$ mm, the **specific** normal $q_{N\,i}$ and shear (tangential) $q_{F\,i}$ contact loads on the i-th section of the plate B will approach the normal σ and shear (tangential) τ contact stresses in this section: $q_{N\,i} \approx \sigma_i$ (MPa), $q_{F\,i} \approx \tau_i$ (MPa).

3. Results and discussion

3.1. Investigation of the contact stresses distribution on the rake surface by the method of a split cutter

Figure 6 shows histograms of specific normal q_{Ni} and shear (tangential) q_{Fi} contact loads on various parts of the rake surface of the cutter, which can be used to plot the distribution (epures, plots) of normal σ and shear (tangential) τ contact stresses.

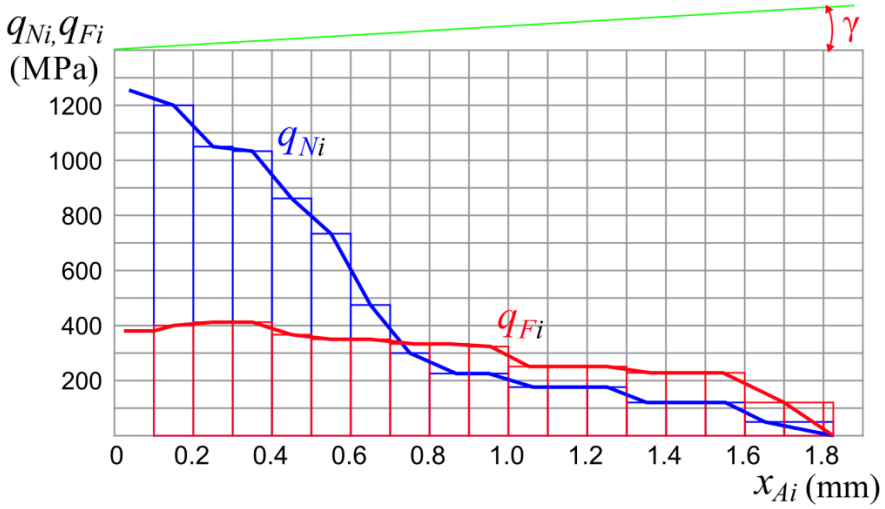

Figure 6. Histograms of specific shear (tangential)q_{Fi} and normal q_{Ni} contact loads (MPa) on the i-th section on the plate B. Abscissa is the distance from the cutting edge $x_{A\,i}$ (mm). Steel 40X – T15K6, $\gamma = +7^{o}$; $v = 120$ m/min; $a = f = 0.368$ mm; $B = 4$ mm; $c = 1.844$ mm; $c_1 = 0.922$ mm; $P_{y\,exp} = 1623$ N; $P_{z\,exp} = 3061$ N; $F_{exp} = 2014$ N; $N_{exp} = 2837$ N.

Plotting is better to start with a plot of shear τ contact stresses, because in Fig. 6 it is possible to distinguish a section from $x_{Ai} = 0$ mm to $x_{Ai} = c_1 = 0.992$ mm (i.e. $c_1 \approx 0.5 \times c$), where the distribution of τ is uniform, i.e. in this section the graph of τ is parallel to the rake surface of the cutter, this corresponds to numerous investigations of contact loads during steel machining [1-4].This will allow you to calculate the magnitude of shear contact stresses τ in this area, knowing the magnitude of the shear force F:

$$\tau_{const} = F/(0{,}75 \cdot c \cdot b). \quad (1$$

where c – is the length of the chip contact with the rake surface (see Figure 2).

In our example, $\tau_{const} = F/(0{,}75 \cdot c \cdot b) = 2014/(0{,}75 \cdot 1{,}84 \cdot 4) = 364{,}9$ (N/mm²). This value corresponds to the average value of shearcontact stresses in this area (τ_i varies from 343 to 400 MPa).

Simplified diagrams of contact stresses are shown in Figure 7. They are also marked with characteristic (reference) points that allow you to draw these diagrams.

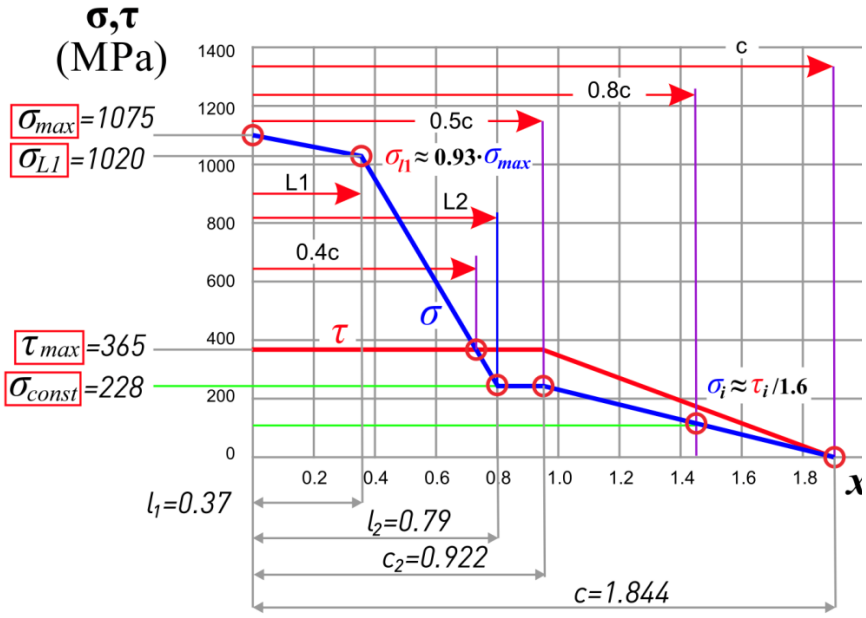

Figure 7. Simplified diagrams of normal **σ** and shear (tangential) **τ** contact stresses (MPa) on the rake (front) surface of the cutter and reference points for their construction. Steel 40X – T15K6, $\gamma = +7^{o}$; $v = 120$ m/min; $a = f = 0.368$ mm; $b = 4$ mm; $c = 1.844$ mm; $c_1 = 0.922$ mm; $P_{y\,exp} = 1623$ N; $P_{z\,exp} = 3061$ N; $F_{exp} = 2014$ N; $N_{exp} = 2837$ N.

The shape of the diagram of normal contact stresses **σ** is much more complicated, therefore we proposed to construct it relative to the diagram of shearcontact stresses **τ**, knowing the change in the conditional coefficient of friction $\mu_i = \tau_i/\sigma_i$ along the rake surface of the cutting tool [9] (Figures 8 and 9).

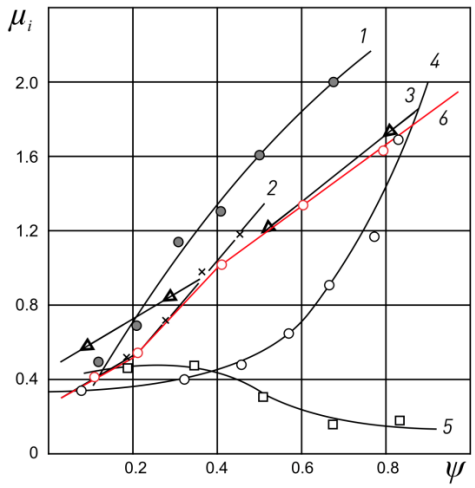

Figure 8. Graphs of changes in the conditional coefficient of friction

$\mu_i = \tau_i / \sigma_i$along the chip contact length depending on the relative coordinate $\psi_i = x_i/c$ according to different authors: 1 – M.F. Poletika and M.H. Uteshev; 2 – G.S. Andreeva and V.M. Zavartseva; 3 – V. Katvinkel; 4 – H. Takeyama and S. Usui; 5 – H. Chandreshekaran and D. Kapoor [9]; 6 – V.N. Kozlov (steel 40X – cemented carbide WC+TiC, a = 0,05–0,368 mm, γ = +35º- 0º).

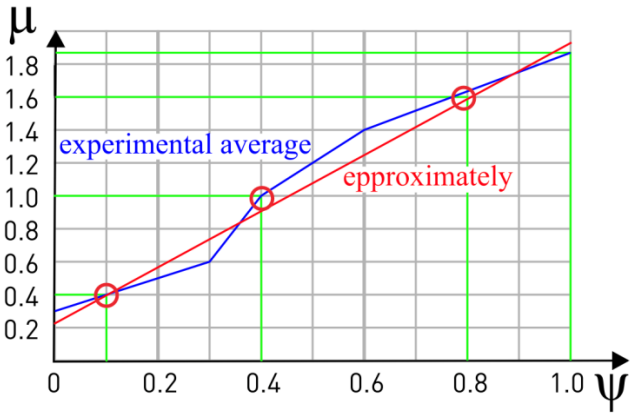

Figure 9. The change in the conditional coefficient of chip friction along the front surface μ_i when machining steel, depending on the relative coordinate $\psi_i = x_i/c$ according to V.N. Kozlov when machining steel 40X with cemented carbide WC+TiC, a = 0,05–0,368 mm, γ = +35º- 0º).

The results of numerous experiments by various researchers have shown that the regularities of the change of the μ_i depend little on the rake angle and the uncut chip thickness $a = s \cdot \sin\varphi$, where φ is the principal edge angle in the plan φ (º) (see figures 1 and 2). When analyzing the experimental results, the relative coordinate $\psi_i = x_i/c$ (dimensionless value) is often used, where x_i is the distance of the point from the cutting edge of the tool.

This allows you to indicate on one graph $c = f(\psi_i)$ the changes of μ at different values of the **uncut chip thickness** a and other cutting conditions, i.e. generalize the results of different experiments in which different chip contact lengths c were obtained.

At the relative coordinate$\psi_i = x_i/c \approx 0.4$, i.e. at $x_i = 0{,}4 \cdot c$, there will be an intersection of the graph σ with the graph τ, because at this point the coefficient of friction $\mu_i = 1$, that is, there $\sigma = \tau$(Figures 7, 8, 9).

At the end of the chip contact with the rake surface of the cutter at the point $\psi_i \approx 0.8$ (i.e. at $x_i \approx 0{,}8 \cdot c$), there should be $\sigma_i \approx t_i / 1.6$ (Figures 7, 8 and 9).

Through two points: number **1** – at $x_i = c$, where $\sigma_i = 0$ MPa; and number **2** at $x_i = 0.8 \cdot c$, where $\sigma_i \approx \tau_i / 1.6$, – we draw a straight line to the intersection of the inclined part of the graph σ with the line perpendicular to the rake surface at point $x_i = 0{,}5 \cdot c$(Figure 7, 10).

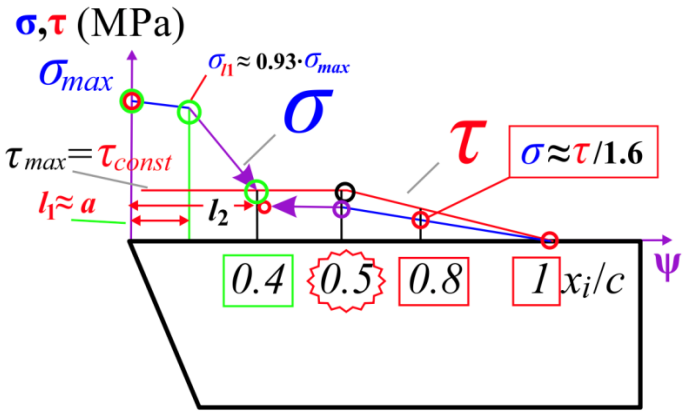

Figure 10. The main reference points for plotting plots and their parameters: τ_{const}, $\sigma_{const} = \sigma_{l2}$, L_2, σ_{max}, σ_{l1}.

From the obtained point, we draw a straight line parallel to the rake surface towards the cutting edge to the intersection with the inclined straight line **σ** falling from the cutting edge (Figure 7, 10), because in the section up to $x_i \approx 0.5 \cdot c$there is a horizontal line at the plot of normal contact stresses **σ**.

The value of σ_{max} at the cutting edge is first we set approximately by ourselves. In the first approximation, $\sigma_{max} = 2 \cdot$**UTS**, where **UTS** is the ultimate tensile stress of the have being machined material at room temperature (MPa). Forexample, forsteel(Fe-0.4 C-1Cr)**UTS** = 495 MPa.

At a distance from the cutting edge $l_1 \approx a$ (mm) $\sigma_{l1} \approx (0.92...0.93) \cdot \sigma_{max}$, because there are no chips there yet, it is just being formed, the pressure from the cutter goes to the workpiece (see Figure 11), so there is an approximately uniform distribution of normal stresses **σ**.

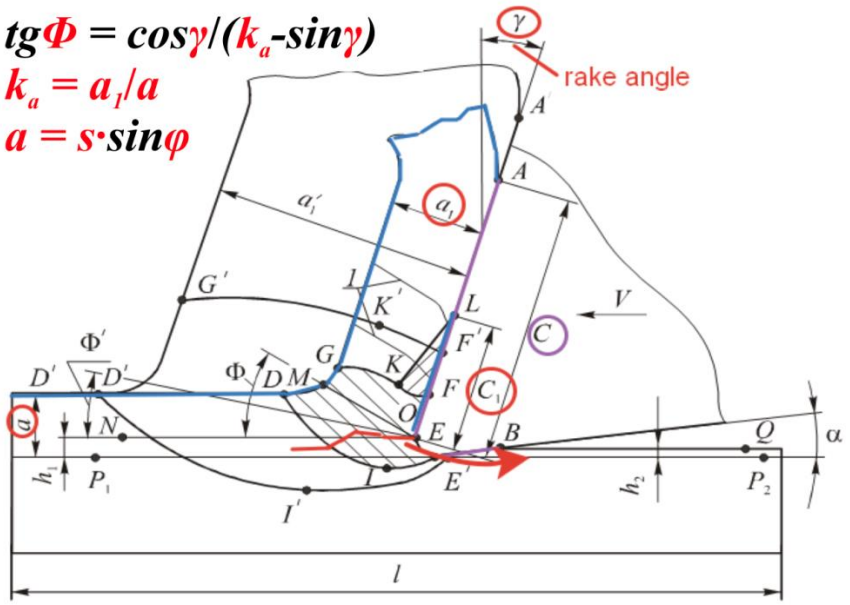

Figure 11. Theprocesses in the chip formation zone in the major orthogonal plane N-N (see Figure 1)

We check the correctness of plotting – the force calculated by the area (volume) of the plot should be approximately equal to the corresponding force from the experiment.

We correct the correctness of the assignment of σ_{max} so that equality is observed

$$N_\sigma = b \times \int_0^c \sigma i \times dx \approx N_{exp}\,(\mathrm{N}), \qquad (1$$

where x varies from 0 (the coordinate at the cutting edge, i.e. at $x = 0$ mm) to $x = c$ (the coordinate of the chip separation point from the rake surface); b is the width of the chip contact with the rake surface of the cutter, for **oblique** cutting $b = t/\sin\varphi$.

To fulfill equality (12), the area of the plot σ (S_σ) is calculated first (see the example in Figure12): $S_\sigma = \Sigma s_{\sigma i}$ (MPa/mm).

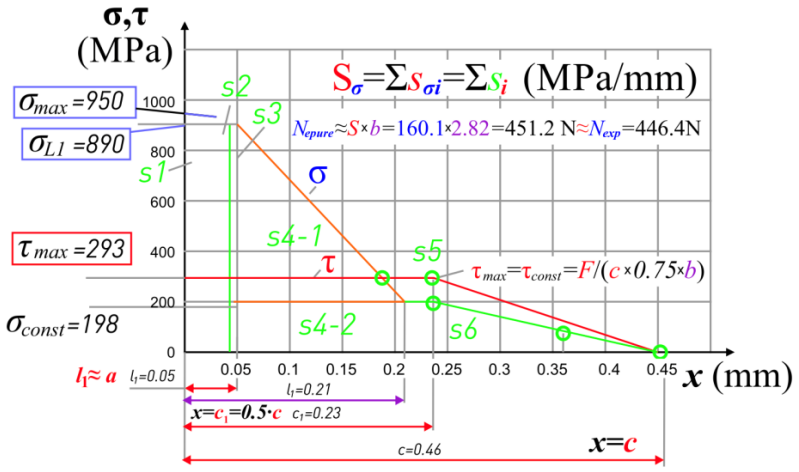

Figure 12. Checking the correctness of plotting normal **σ** and shear **τ** contact stresses on the rake surface of the cutter during **oblique** cutting. Steel 40X - T15K6; t = 2 mm; v = 120 m/min; γ = 7 º, φ = 45º, f = 0.07 mm/rev.

Then the normal force is calculated from the plot **σ**: $N_\sigma = S_\sigma \cdot b$ (N). It should be approximately equal to the normal force according to the experiment N_{exp} (N).

If the normal force according to the plot **σ**, i.e. N_σ, is less than the one obtained in the experiment N_{exp}, then we increase σ_{max}, if more – then we decrease it. After that, we recalculate the normal force according to the plot N_σ and repeat until we get $N_\sigma \approx N_{exp}$.

Similarly, we perform for the shear force according to the plot **τ**: $F_\tau = S_\tau \cdot b \approx F_{exp}$ (N).

But there shouldn't be any problems here, because initially $\tau_{const} = F/(0{,}75 \cdot c \cdot b)$.

Finding the value of σ_{max} by the above method is the only possible way to determine it, because no currently known method can determine contact stresses closer than 0.1-0.2 mm from the cutting edge, because the plates A and B of the split cutter (Figure 3) are being chipped if the distance from the cutting edge to the separation surface of the plates $x_{Ai} \leq 0.2$ mm, and when using laser interferometry methods [11-13] or polarization-optical [1], the lines (strips) of isocline or isochrome merge and it is impossible to distinguish them.

3.2. *Determination of the influence of cutting conditions on the value of the main parameters of the contact stress diagrams on the rake surface after measuring the technological components of the cutting force with a Kistler dynamometer*

The technological components P_z, P_x and P_y of the cutting force (see Figure 1) were measured during longitudinal turning of a workpiece

made from steel 40X with a conventional turning cutter mounted on a three-component Kistler turning dynamometer.

Cutting was carried out with a different feed rate $f = 0.07$ ... 0.52 (mm/rev) at a cutting speed $v = 120$ m/min, which excluded the appearance of a built-up-end (growth) on the rake surface of the cutter. The magnitude of the side-rake angle γ varied from +40 to -10°.

After cutting, the total chip contact length c (mm) and the length of the plastic chip contact c_1 (mm) with the rake surface were measured using an instrumental portable microscope (Figures 2, 12). Graphs of the effect of the uncut chip thickness a and the rake angle γ on the total chip contact length c, which is necessary for plotting contact stresses, were constructed (Figure 13).

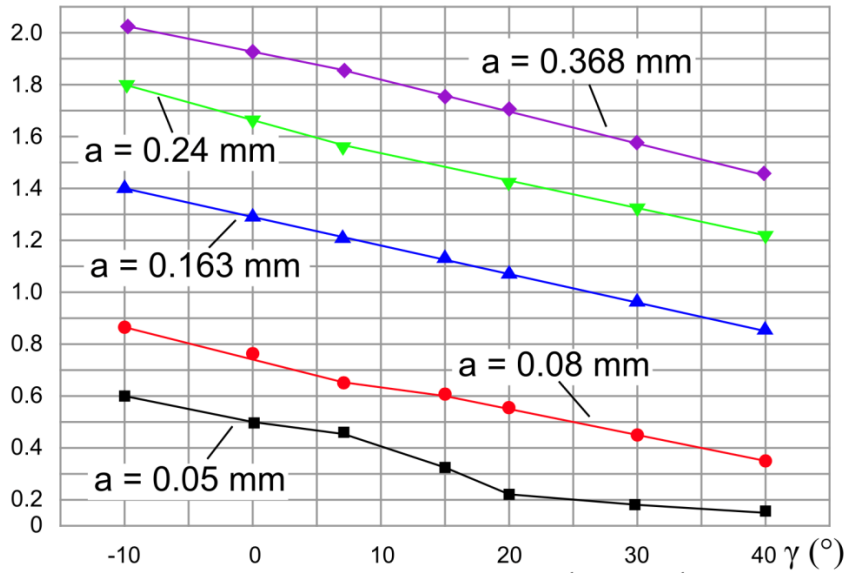

Figure 13. Graphs of the change of the total chip contact length c (mm) with the rake surface of the cutter depending on the side-rake angle γ (°) and the uncut chip thickness a (mm) at φ = 45°.

A chamfer with a length $h_f = 0.95$ mm with the clearance (flank, rear, side-relief) angle $\alpha_h = 0$ º was sharpened on the side-relief (rear, flank, back) surface to study the effects of wear on the technological components of the cutting force. It simulated wear on the side-relief surface. After carry out a series of experiments with different feed rates f, the cutter was re-sharpened only along the side-relief surface with a side-relief (rear, **clearance**) angle $\alpha = 12$ °, which ensured a constant side-relief angle on the chamfer $\alpha_h = 0$ º when the length of the chamfer h_f was varied from 0.95 mm to zero, i.e. to a sharp cutter.

By extrapolating the components P_z, P_x and P_y of the cutting force to the zero wear chamfer, forces acting only on the rake surface of P_{zr}, P_{xr} and P_{yr} were isolated. The resulting component $P_{xy_r} = \sqrt{P_{xr}^2 + P_{yr}^2}$, acting in the reference (main) plane was calculated. These components P_{xyr} and P_{zr} were used to calculate the normal N and shear F of the physical components of the cutting force on the rake surface according to equations (3) and (4) with a negative value of the rake angle γ, and with a positive value of the rake angle γ, equations (13) and (14) were used:

$$N = N_{Pz} - N_{Pxy} = P_{zr} \times \cos\gamma - P_{xyr} \times \sin\gamma, \quad (1$$

$$F = F_{Pxy} + F_{Pz} = P_{xyr} \times \cos\gamma + P_{zr} \times \sin\gamma. \quad (1$$

Based on these physical components N and F of the cutting force, plots of normal **σ** and shear **τ** contact stresses on the rake surface were constructed, taking into account the **regularities** (patterns) which were

obtained by the split cutter method. On each graph of the distribution of contact stresses, the values of the main parameters of the plots (reference points) were determined (Figure 10), after which graphs of the effect of the uncut chip thickness $a = f \cdot \sin\varphi$ (mm) and the rake angle γ (º) (cutting conditions) on the value of the main parameters of the plots of contact stresses on the rake (front) surface were plotted in turning of steel 40X (Figures 10, 12, 13, 14). A large number of points on the graphs allows us to confidently assert the reliability of the obtained graphs.

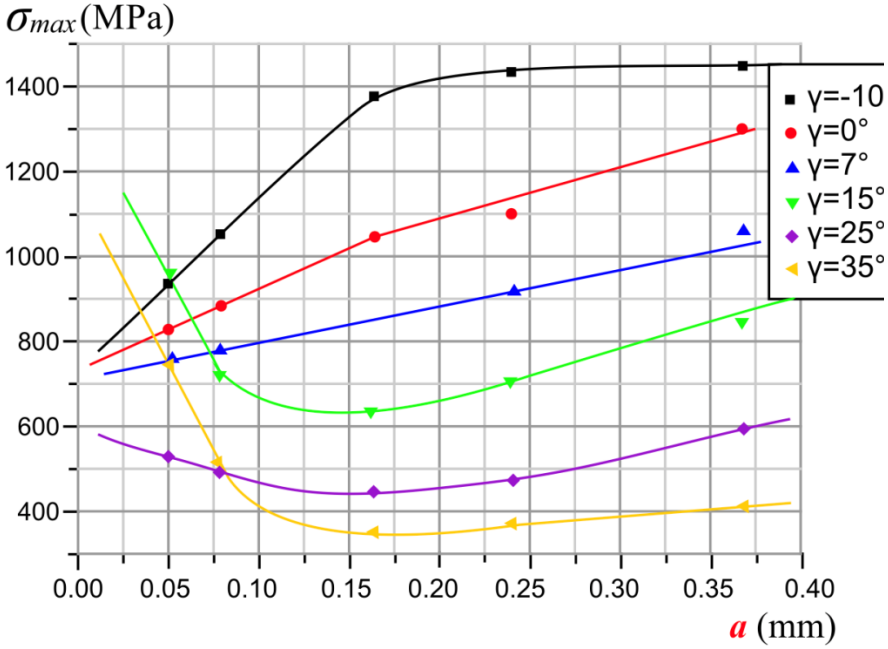

Figure 14. The effect of the uncut chip thickness*a* and the rake angle γ on the value of the highest normal contact stress σ_{max} on the rake surface when machining steel 40X.

The greatest interest are the graphs of the effect of the uncut chip thickness ***a*** and the rake angle γ on the largest normal contact stress σ_{max} on the rake surface (Figure 14), since this value determines the load on the rake surface of an unworn out cutting tool.

It can be seen from the graphs in Figure 14 that a decrease in the rake angle γ from +35 to -10 ° leads to a significant increase in σ_{max} from 400 to 1400 N with the uncut chip thickness a = 0,368 mm. When the uncut chip thickness*a* decreases in the range from 0.368 to 0.17 mm, the value of σ_{max} decreases, which also does not cause contradictions with existing ideas about contact processes on the rake surface.

With the uncut chip thickness ***a***less than 0.17 mm, σ_{max} begins to decrease intensively at γ = -10 °, but on the contrary it increases at γ = +35 °, +25 ° and +15 °.

In our opinion, the intensive decrease in σ_{max} at γ = - 10º and the small uncut chip thickness ($a < 0.15$ mm) is associated with the appearance of a small **build-up-edge** (growth) on the rake surface and an increase in the actual the rake angle γ[1]. With a large uncut chip thickness ***a***, this effect is not so significant.

The second factor contributing to a decrease in σ_{max} at γ = -10 ° and $a < 0.15$ mm is associated with an increase in the deflection (sag) of the transient (cutting) surface [5], which leads to a decrease in pressure on the rounded section of the cutting edge due to the redistribution of the normal load on the rest of the chip contact with the rake surface.

Therefore, the paradoxical intensive increase in σ_{max} at γ = +35 ° and a small uncut chip thickness $a < 0.17$ mm is also associated, in our opinion,

with the deterioration of conditions for the formation of a small build-up-edge: with $\gamma > +25$ ° the probability of the appearance of the build-up-edge (growth) decreases sharply [1]. The appearance of the build-up-edge causes an increase in the actual rake angle γ_{actual}, and this leads to a decrease in the cutting force [1].

The presence of a small build-up-edge is especially important when machining with a small uncut chip thickness a, because the build-up-edge prevents the indentation (pressing) of the have being machined material under the cutting edge (see Figure 11) [1-2], which means it prevents a significant increase in forces on the radius section of the rounded cutting edge: even with a sharpened cutter, the radius of rounding of the cutting edge is $\varrho \approx 0.002$-0.005 mm.

With a small chip thickness ($a < 0.17$ mm), the indentation (pressing) of the have being machined material under the cutting edge in the chip formation zone increases [1]. This leads to an increase in the components of the cutting force $P_{z\varrho}$, $P_{y\varrho}$ and $P_{x\varrho}$ on a rounded section of the cutting edge, but in the absence of a wear chamfer on the flank surface, this is perceived as forces on a flat area of the rake surface.

The increase in σ_{max} at $\gamma = +15$ º and a smallvalue of the uncut chip thickness ($a < 0.1$ mm) is similar to the changes at $\gamma = +35$ °, but begins a little later with a decrease in the uncut chip thickness due to a smaller rake angle. A similar effect should be at $\gamma = +25$ º with a decrease in the uncut chip thickness $a < 0.14$ mm, however, a not very intense increase in σ_{max} compared to $\gamma = +15$ º is unclear and can only be explained by us as an error in measuring forces at $a = 0.05$ mm with the rake angle $\gamma = +25$ º.

Special attention should also be paid to the effect of the uncut chip thickness a on the value of the greatest shear contact stress $\tau_{max} = \tau_{const}$ (Fig. 15). These graphs confirm the statements of various researchers about the small effect of the uncut chip thickness a and the rake angle γ on its magnitude [1]. Only when the rake (front) angle $\gamma = -10$ ° is negative, the graph $\tau_{max} = f(a)$ differs from the others.

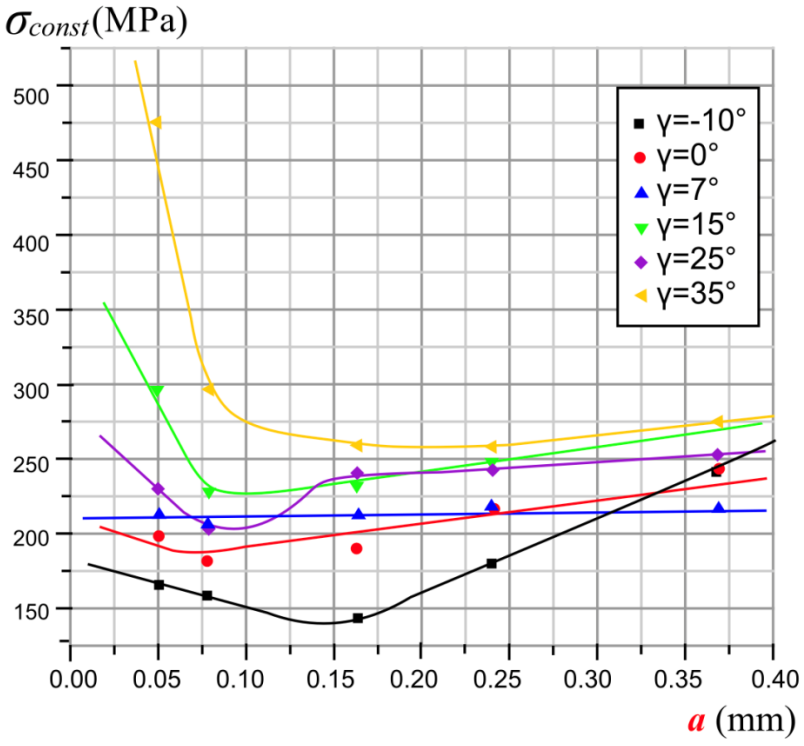

Figure 15. The effect of the uncut chip thickness a and the rake angle γ on the magnitude of the greatest shear contact stress τ_{max} on the rake surface when machining steel (Fe-0.4 C-1Cr).

The value of the greatest shear stress $\tau_{max} = \tau_{const}$ varies slightly (τ_{max} = 350-400 MPa) in the range of the uncut chip thickness a = 0.37-0.07 mm and the rake angle γ = +35-0 °, but the greater the rake angle γ, the greater the value of the τ_{max}. At γ = +7 °, the value of τ_{max} does not change, which allowed scientists to assert that the cutting mode does not affect the value of the shear stress τ on the first half of the chip contact length.

Increase in τ_{max} at a small value of the uncut chip thickness a < 0.07 mm for γ = +35 … +15 º is explained by us as the effect of indentation (pressing) of the being machined material under the cutting edge in the chip formation zone, what causes an increase in forces not on a flat area of the rake surface, but on the rounded section of the cutting edge: the larger the rake angle, the more intensively the τ_{max} increases in this area with a decrease in the uncut chip thickness a < 0.07 mm.

The special character of the graph $\tau_{max} = f(a)$ at γ = -10 º is explained by us as the influence of a seizure (stagnant) zone or a build-up-edge: at a negative rake angle, the velocity vector of the have being formed chips changes its direction, which creates more favorable conditions for the formation of a seizure (stagnant) zone. With a decrease in the uncut chip thickness a < 0.37 mm, even its small value more significantly changes the friction force on the contact surface at the cutting edge.

With a further decrease in the uncut chip thickness (a < 0.17 mm), an increase in τ_{max} occurs due to an increase in forces not on a flat area of the rake surface, but on the rounded section of the cutting edge due to the indentation (pressing) of the have being machined material under the cutting edge in the chip formation zone, which occurs to a greater extent with a negative rake angle.

5. Conclusions

1. Investigation of the distribution of contact stresses on the rake surface of the cutter by the split cutter method when machining 40X steel revealed characteristic (reference) points on the plots of normal σ and tangential τ contact stresses, which are necessary for plotting when machining steel 40X (Fe-0.4 C-1Cr). These characteristic points can be used for plotting when machining steel of other grades, alloys, as well as other materials, during the machining of which **continuous** chips being formed.
2. The effect of the **uncut chip thickness** $\boldsymbol{a}$ and the rake angle $\boldsymbol{\gamma}$ on the total length of the chip contact with the rake surface $\boldsymbol{c}$ was revealed during the machining 40X steel. Graphs were constructed and equations were obtained for calculating the chip contact length $\boldsymbol{c}$.
3. When plotting contact stresses on the rake surface of the cutting tool when machining steel, it is necessary to start with plotting shear contact stresses $\boldsymbol{\tau}$, because it has a simpler form, which allows using a simple formula to determine its main parameter, $\boldsymbol{\tau_{max} = \tau_{const} = F/(0{,}75 \cdot c \cdot b)}$.
4. The shape of the diagram (epures) of normal contact stresses $\boldsymbol{\sigma}$ is much more complicated, therefore we proposed to construct it relative to the diagram of shear (tangential)contact stresses $\boldsymbol{\tau}$, knowing the change in the conditional coefficient of friction $\boldsymbol{\mu_i = \tau_i/\sigma_i}$ along the rake (front) surface of the cutting tool.
5. The results of numerous experiments by different researchers have shown that the **regularities** of the change of $\boldsymbol{\mu}$ depend little on the rake (front) angle $\boldsymbol{\gamma}$ and the **uncut chip thickness** $\boldsymbol{a}$. When

analyzing the experimental results, the relative coordinate $\psi_i = x_i/c$ was used.

6. After plotting the contact stresses epures, it is necessary to check the correctness of their construction – the force calculated by the volume of the plot should be approximately equal to the corresponding force from the experiment.
7. The values of its main parameters (reference points) (σ_{max}, σ_{const}, L_2, τ_{max}) were determined on each plot (epure), after which graphs of the effect of the **uncut chip thickness** $a = f \cdot \sin\varphi$ (mm) and the rake (front) angle γ (º) on their value when turning steel 40X were constructed. A large number of points on the graphs allows us to confidently assert the reliability of the obtained graphs.
8. In machining steel 40X (Fe-0.4 C-1Cr) the greatest normal contact stress on a rake surface $\sigma_{max} \approx$ 500-1100 MPa depends on **uncut chip thickness** a and **rake** angle γ;
9. A decrease in the **rake** angle γ from +35 to -10° leads to a significant increase in σ_{max} from 400 to 1400 MPa for the **uncut chip thickness** a = 0.368 mm, which does not cause contradictions with existing ideas about contact processes on the **rake** surface. It is also natural decreasing σ_{max} with a decrease in the **uncut chip thickness** a in the range from 0.368 to 0.17 mm.
10. The paradoxical intensive increase in σ_{max} at γ = +35 - +15 ° with a decrease in the **uncut chip thickness** a < 0.17 mm is associated, in our opinion, with an increase in the indentation (pressing) of have being formed material under the cutting edge in the chip formation zone. This leads to an increase in the components of the cutting force $P_{z\varrho}$, $P_{y\varrho}$ and $P_{x\varrho}$ on the rounded section of the cutting edge with radius ϱ, but in the absence of a wear chamfer on the flank (back) surface, this is perceived as forces on a flat area of the rake (front) surface.
11. The value of the greatest shear (tangential) stress $\tau_{max} = \tau_{const}$ varies slightly (τ_{max} = 350-400 MPa) in the range of the **uncut chip thickness** a = 0.37-0.07 mm and the rake (front) angle γ = +35-0 °, but the greater the rake (front) angle γ, the greater the value of the τ_{max}. At γ = +7 °, the value of τ_{max} does not change, which allowed scientists to assert that the cutting mode does not affect the value of the shear (tangential) stress τ on the first half of the chip contact length.
12. In machining steel 40X (Fe-0.4 C-1Cr) a medium (an average) conditional coefficient of friction on a rake surface is large $\mu_m \approx$ 0.6-0.8. It leads to occurrence of essential radial force on a rake surface P_{xyr} (force P_{yr} in orthogonal free cutting) and leads a sag (deflection) of a transient surface. The presence of the sag (deflection) of the transient surface leads to a decrease in contact stresses on the side-relief (rear, flank, back) surface or on the wear chamfer on the side-relief (rear, flank, back) surface near the cutting edge when machining materials forming continuous chips.

Author Contributions: Conceptualization, V.K., A.B; methodology, A.B., A.S.; validation, V.K., A.B.; formal analysis, V.K., A.B.; investigation, V.K., A.B., N.S.; resources, N.S., A.Sh.; writing—original draft preparation, V.K.; writing—review and editing, A.B., N.S., A.S.; visualization, A.Sh., A.S.; supervision, V.K., A.B., N.S.All authors have read and agreed to the published version of the manuscript.

Funding: This research was funded by the Russian Science Foundation, project No. 23-79-10166.

Data Availability Statement: The data presented in this study are available upon request from the corresponding author

Acknowledgments: The research was carried out with the equipment of the Tomsk Regional Core Shared Research Facilities Center of National Research Tomsk State University and using the equipment of the Center for Collective Use "Nanomaterials and Nanotechnologies" of the Tomsk Polytechnic University, for access to which the authors are grateful

Conflicts of Interest: The authors declare no conflict of interest.

Nomenclature

a	uncut chip thickness (mm) a1 chip thickness (mm)
Ka	chip thickness ratio, Ka = a_1/a
φ	the major cutting edge angle (degree, ◦)
φ_1	the minor cutting edge angle (degree, ◦)
t	depth of cut (mm)
v	cutting speed (m/min)
γ	rake angle (degree, ◦)
α	the clearance angle—the angle between the flank (or tangent to it) and the cutting edge plane (degree, ◦)
c	tool-chip length (the length of the chip contact with the rake surface) (mm)
c_1	tool-chip sticking zone length (mm)
l_2	tool-chip slipping zone length (mm)
ϱ	radius of rounding of the cutting edge (mm)
τ	shear stress on the rake surface (MPa)
τ_{max}	the greatest value of the shear stress on the rake surface (MPa)
σ_{max}	the greatest value of the normal stress on the rake surface (MPa)
σ	normal stress on the rake surface (MPa)
μ	conditional coefficient of friction on the rake surface
f	feed rate (mm/rev)

References

1. F. Klocke, W. Lortz, D. Trauth. Analysis of the dynamic chip formation process in turning **2018** Volume 135, 313-324.https://doi.org/10.1016/j.ijmecsci.2017.11.035
2. A.Gouarir, G. Martínez-Arellano, G. Terrazas, P. Benardos, S. Ratchev. In-process Tool Wear Prediction System Based on Machine Learning Techniques and Force Analysis *Journal of Procedia CIRP*, **2018**, Volume 77, Pages 501-504.https://doi.org/10.1016/j.procir.2018.08.253
3. Díaz-Álvarez, J.; Díaz-Álvarez, A.; Miguélez, H.; Cantero, J.L. Finishing Turning of Ni Superalloy Haynes 282. *Metals***2018**, *8*, 843.https://doi.org/10.3390/met8100843
4. Grzesik, W.; Niesłony, P.; Habrat, W.; Sieniawski, J.; Laskowski, P. Investigation of tool wear in the turning of Inconel 718 superalloy in terms of process performance and productivity enhancement. *Tribol. Int.* **2018**, *118*, 337–346https://doi.org/10.1016/j.triboint.2017.10.005
5. Hoier, P.; Malakizadi, A.; Stuppa, P.; Cedergren, S.; Klement, U. Microstructural characteristics of Alloy 718 and Waspaloy and their influence on flank wear during turning. *Wear* **2018**, 400, 184–193.https://doi.org/10.1016/j.wear.2018.01.011
6. Mehmet Erdi Korkmaz, NafizYaşar, Mustafa Günay. Numerical and experimental investigation of cutting forces in turning of Nimonic 80A superalloy. *Engineering Science and Technology, an International Journal***2020**, Volume 23, Issue 3, Pages 664-673.https://doi.org/10.1016/j.jestch.2020.02.001
7. Ramanuj Kumar, Ashok Kumar Sahoo, Purna Chandra Mishra & Rabin Kumar Das. Advances in Manufacturing **2018**, 6, 52–70.https://link.springer.com/article/10.1007/s40436-018-0215-z
8. Samarjit Swain, IshamPanigrahi, Ashok Kumar Sahoo, Amlana Panda &Ramanuj Kumar. Effect of Tool Vibration on Flank Wear and Surface Roughness During High-Speed Machining of 1040 Steel. *Journal of Failure Analysis and Prevention***2020**, 20, 976–994.https://doi.org/10.1007/s11668-020-00905-x
9. G. Jangali Satish, V.N. Gaitonde, Vinayak N. Kulkarni. Traditional and non-traditional machining of nickel-based superalloys: A brief review. *Materials today proceedings***2021**, Volume 44, Part 1, 1448-1454.https://doi.org/10.1016/j.matpr.2020.11.632

10. Victor Kozlov, Jia Yu Zhang, Ying Bin Guo, Sai Kiran Sabavath. *High Technology: Research and Applications***2018**, Volume 769, 284-289.https://doi.org/10.4028/www.scientific.net/KEM.769.284
11. Mohsen Marani, MohammadjavadZeinali, Jules Kouam, Victor Songmene& Chris K. Mechefske. Prediction of cutting tool wear during a turning process using artificial intelligence techniques**.** *The International Journal of Advanced Manufacturing Technology***2020**, 111, 505–515.https://doi.org/10.1007/s00170-020-06144-6
12. Natalia Szczotkarz, Roland Mrugalski, Radosław W. Maruda, Grzegorz M. Królczyk, StanisławLegutko, Kamil Leksycki, Daniel Dębowski, Catalin I. Pruncu. Cutting tool wear in turning 316L stainless steel in the conditions of minimized lubrication. *Tribology International***2021**, Volume 156, 106813.https://doi.org/10.1016/j.triboint.2020.106813
13. JinfuZhaoab, ZhanqiangLiuab, BingWangc, JianruiHuab, Yi Wanab. Tool coating effects on cutting temperature during metal cutting processes: Comprehensive review and future research directions. *Mechanical Systems and Signal Processing***2021**, Volume 150, 107302.https://doi.org/10.1016/j.ymssp.2020.107302
14. Zhaopeng He, Tielin Shi, Jianping Xuan, Tianxiang Li. Research on tool wear prediction based on temperature signals and deep learning. *Wear***2021**, Volumes 478–479, 203902.https://doi.org/10.1016/j.wear.2021.203902
15. Hongguang Liu, Xiang Xu, Jun Zhang, Zhechao Liu, Yong He, Wanhua Zhao, Zhanqiang Liu. The state of the art for numerical simulations of the effect of the microstructure and its evolution in the metal-cutting processes. *International Journal of Machine Tools and Manufacture***2022**, Volume 177,103890.https://doi.org/10.1016/j.ijmachtools.2022.103890
16. Toukir Ahmed, NriponMollick, Shahed Mahmud, Tareq Ahmad Analysis of Effects of Machining Parameters on Cutting Force Components in Turning AISI 201 Stainless Steel Using Cemented Carbide Cutting Tool Insert. *Materials Today: Proceedings* **2021**, Volume4 2, Part 2, 832-837.https://doi.org/10.1016/j.matpr.2020.11.416
17. Kadir Gok. Development of three-dimensional finite element model to calculate the turning processing parameters in turning operations. *Measurement***2015**, Volume 75,57-68.https://doi.org/10.1016/j.measurement.2015.07.034
18. Kejia Zhuang, Changni Fu, Jian Weng & Cheng Hu Cutting edge microgeometries in metal cutting: a review. *The International Journal of Advanced Manufacturing Technology***2021**, 116, 2045–2092.https://doi.org/10.1007/s00170-021-07558-6
19. Chetan, Sudarsan Ghosh, P. Venkateswara Rao. Application of sustainable techniques in metal cutting for enhanced machinability: a review. Journal of Cleaner Production 2015, Volume 100,17-34.https://doi.org/10.1016/j.jclepro.2015.03.039
20. Ali Hosseini & Hossam A. Kishawy. Cutting Tool Materials and Tool Wear. *Machining of Titanium Alloys***2014**, 31-56.https://doi.org/10.1007/978-3-662-43902-9_2
21. WafaaRmili, AbdeljalilOuahabi, Roger Serra, René Leroy. An automatic system based on vibratory analysis for cutting tool wear monitoring. *Measurement***2016**, Volume 77,117-123. https://doi.org/10.1016/j.measurement.2015.09.010
22. M. Rizal, J.A. Ghani, M.Z. Nuawi, C.H.C. Haron. Cutting tool wear classification and detection using multi-sensor signals and Mahalanobis-Taguchi System. *Wear***2017**, Volumes 376–377, Part B, 15, 1759-1765.https://doi.org/10.1016/j.wear.2017.02.017
23. Yan Shen, Feng Yang, Mohamed Salahuddin Habibullah, Jhinaoui Ahmed, Ankit Kumar Das, Yu Zhou &Choon Lim Ho. Predicting tool wear size across multi-cutting conditions using advanced machine learning techniques. *Journal of Intelligent Manufacturing***2021**, volume32, 1753–1766.https://doi.org/10.1007/s10845-020-01625-7
24. Mehdi Nouri, Barry K. Fussell, Beth L. Ziniti, Ernst Linde. Real-time tool wear monitoring in milling using a cutting condition independent method. *International Journal of Machine Tools and Manufacture***2015**, Volume 89, 1-13.https://doi.org/10.1016/j.ijmachtools.2014.10.011
25. Shao-Hsien Chen &Zhi-Rong Luo. Study of using cutting chip color to the tool wear prediction. *The International Journal of Advanced Manufacturing Technology***2020**, 109,823–839.https://doi.org/10.1007/s00170-020-05354-2
26. Pradeep V. Badiger, Vijay Desai, M. R. Ramesh, B. K. Prajwala& K. Raveendra. Cutting Forces, Surface Roughness and Tool Wear Quality Assessment Using ANN and PSO Approach During Machining of MDN431 with TiN/AlN-Coated Cutting Tool. *Arabian Journal for Science and Engineering***2019**, volume44, 7465–7477.https://doi.org/10.1007/s13369-019-03783-0
27. F. Salvatore, S. Saad, H. Hamdi. Modeling and Simulation of Tool Wear During the Cutting Process. *Procedia CIRP***2013**, Volume 8,305-310.https://doi.org/10.1016/j.procir.2013.06.107
28. A. Kannan, R. Mohan, R. Viswanathan, N. Sivashankar. Experimental investigation on surface roughness, tool wear and cutting force in turning of hybrid (Al7075 + SiC + Gr) metal matrix composites. *Journal of Materials Research and Technology***2020**, Volume 9, Issue 6, 16529-16540.https://doi.org/10.1016/j.jmrt.2020.11.074

29. Ch. Shoba, N. Ramanaiah, D. Nageswara Rao. Effect of reinforcement on the cutting forces while machining metal matrix composites–An experimental approach. *Engineering Science and Technology, an International Journal***2015**, Volume 18, Issue 4, 658-663.https://doi.org/10.1016/j.jestch.2015.03.013
30. Wang Sujuan, Zhang Tao, Deng Wenping, Sun Zhanwen& Sandy To. Analytical modeling and prediction of cutting forces in orthogonal turning: a review. *The International Journal of Advanced Manufacturing Technology***2022**, 119, 1407-1434.https://doi.org/10.1007/s00170-021-08114-y
31. N R Dhar, Nanda S V Kishore, and A B Chattopadhyay. The effects of cryogenic cooling on chips and cutting forces in turning AISI 1040 and AISI 4320 steels. *Proceedings of the Institution of Mechanical Engineers, Part B: Journal of Engineering Manufacture* 2012, Volume 216, Issue 5.http://dx.doi.org/10.1243/0954405021520409
32. B.Tulasiramarao , Dr.K.Srinivas , Dr. P Ram Reddy , A.Raveendra , Dr.B.V.R.Ravi Kumar. Finding Cutting Forces While Turning Aperation on Lathe Machine at Different Depth of Cut of Different Metals. *International Journal of Innovative Research in Science, Engineering and Technology***2014**, Vol. 3, Issue 10. http://dx.doi.org/10.15680/IJIRSET.2014.0310065
33. V. P. Lapshin, I. A. Turkin& V. V. Khristoforova. Assessment of Metal Wear in Turning on the Basis of Components of the Cutting Force. *Russian Engineering Research***2020**, 40, 797–800.https://doi.org/10.3103/S1068798X20090099
34. ItxasoCascón, Jon Ander Sarasua. Mechanistic Model for Prediction of Cutting Forces in Turning of Non-axisymmetric Parts. *Procedia CIRP***2015**, Volume 31, 435-440.https://doi.org/10.1016/j.procir.2015.03.084
35. Rityuj Singh Parihar, Raj Kumar Sahu, G. Srinivasu. Finite Element Analysis of Cutting Forces Generated in Turning Process using Deform 3D Software. *Materials today proceedings***2017**, Volume 4, Issue 8, 8432-8438.https://doi.org/10.1016/j.matpr.2017.07.188
36. S. Sai Venkatesh, T. A. Ram Kumar, A. P. Blalakumhren, M. Saimurugan, and K. Prakash Marimuthu. Finite element simulation and experimental validation of the effect of tool wear on cutting forces in turning operation. *Mechanics and Mechanical Engineering***2019**, 23:297-302.http://dx.doi.org/10.2478/mme-2019-0040